

RESEARCH ARTICLE

The T cell IFT20 interactome reveals new players in immune synapse assembly

Donatella Galgano¹, Anna Onnis¹, Elisa Pappalardo², Federico Galvagni³, Oreste Acuto² and Cosima T. Baldari^{1,*}

ABSTRACT

Sustained signalling at the immune synapse (IS) requires the synaptic delivery of recycling endosome-associated T cell antigen receptors (TCRs). IFT20, a component of the intraflagellar transport system, controls TCR recycling to the IS as a complex with IFT57 and IFT88. Here, we used quantitative mass spectrometry to identify additional interaction partners of IFT20 in Jurkat T cells. In addition to IFT57 and IFT88, the analysis revealed new binding partners, including IFT54 (also known as TRAF3IP1), GMAP-210 (also known as TRIP11), Arp2/3 complex subunit-3 (ARPC3), COP9 signalosome subunit-1 (CSN1, also known as GPS1) and ERGIC-53 (also known as LMAN1). A direct interaction between IFT20 and both IFT54 and GMAP-210 was confirmed in pulldown assays. Confocal imaging of antigen-specific conjugates using T cells depleted of these proteins by RNA interference showed that TCR accumulation and phosphotyrosine signalling at the IS were impaired in the absence of IFT54, ARPC3 or ERGIC-53. Similar to in IFT20-deficient T cells, this defect resulted from a reduced ability of endosomal TCRs to polarize to the IS despite a correct translocation of the centrosome towards the antigen-presenting cell contact. Our data underscore the traffic-related role of an IFT20 complex that includes components of the intracellular trafficking machinery in IS assembly.

KEY WORDS: Mass spectrometry analysis, Intraflagellar transport system, Immune synapse assembly

INTRODUCTION

Engagement of the T cell antigen receptor (TCR) by cognate peptide major histocompatibility complex (pMHC) triggers the assembly of the immunological synapse (IS), a dynamic supra-molecular membrane structure formed at the contact between the T cell and antigen-presenting cell (APC) (Kumari et al., 2014; Fooksman et al., 2010). In addition to organizing signal propagation, the IS likely participates in signal processing required for adequate T cell activation (Acuto et al., 2008). Over the last decade, intracellular membrane trafficking has been recognized as a key mechanism in the assembly and the function of IS, where it contributes to regulate signal intensity and duration by controlling the amount and dwell time of receptors and signalling mediators at the T cell–APC interface. The synaptic accumulation of endosomal vesicles containing TCRs, as well as other proteins that undergo cycles of

internalization and re-expression, is achieved by polarized endosome recycling (Das et al., 2004; Soares et al., 2013a; Finetti and Baldari, 2013). Once delivered in the proximity of the IS environment, the TCRs continue to recycle between the plasma membrane and the recycling compartment. This ensures a continuous supply of endosome-associated receptors to the IS, until signalling is shut off as a result of their lysosomal degradation (Das et al., 2004). Other receptors, such as the transferrin receptor (TfR), CD28, LFA-1 (lymphocyte function-associated antigen 1, a complex between integrin α L and integrin β 2), GLUT-1 (also known as SLC2A1) and CTLA-4 exploit the recycling pathway to move in or out of the IS (Yokosuka et al., 2008; Piotrowski et al., 2013; Finetti and Baldari, 2013; Egen and Ellison, 2002). Two key membrane-associated TCR signalling regulators, the kinase Lck and the transmembrane scaffold LAT, exist as two pools, one of which is associated with the plasma membrane and the other with recycling endosomes that translocate to the T-cell–APC interface in response to stimulation (Ley et al., 1994; Bonello et al., 2004; Ehrlich et al., 2002; Larghi et al., 2013; Soares et al., 2013b). Observations made by super-resolution microscopy show that, similar to the compartmentalization in distinct nanodomains of their surface counterparts (Lillemeier et al., 2010; Williamson et al., 2011; Sherman et al., 2011; Rossey et al., 2013), vesicular CD3 ζ (also known as CD247), LAT and Lck are associated with distinct exocytic compartments marked by specific sets of Rab proteins, and are released at the IS in a differentially regulated manner (Soares et al., 2013b). It has been speculated that fusion at the IS of vesicles carrying these signalling molecules can generate nanoterritories that function as hubs for signal amplification (Soares et al., 2013b).

The diversification and complexity of the intracellular trafficking pathways converging to the IS poses a major challenge in dissecting the underlying mechanisms and identifying the dedicated proteins for each pathway. We have previously demonstrated that the IFT20, a component of intraflagellar transport (IFT) system, which is responsible for the assembly of the primary cilium in other cells, controls TCR accumulation at the IS in the non-ciliated T cell as a complex with IFT52, IFT57 and IFT88 (Finetti et al., 2009, 2014). This function involves the participation of IFT20 in the pathway that orchestrates polarized receptor recycling to the IS, with IFT20 interacting with the small GTPase Rab5 to promote the transit of internalized TCRs and TfRs from early to recycling endosomes (Finetti et al., 2009, 2014). Interestingly, we identified two other small GTPases, Rab8, a master regulator of ciliogenesis (Nachury et al., 2011), and Rab29, which is involved in *Salmonella*-containing vacuole trafficking in infected epithelial cells (Spanò et al., 2011), as central players in the TCR recycling pathway orchestrated by IFT20 and Rab11 (note that Rab5, Rab8 and Rab11 have more than one isoform, but we do not refer to a specific form here) (Finetti et al., 2015; Onnis et al., 2015). Of note, both Rab8 and Rab29 are dispensable for TfR recycling, while they are

¹Department of Life Sciences, University of Siena, Siena 53100, Italy. ²Sir William Dunn School of Pathology, University of Oxford, Oxford OX1 3RE, UK. ³Department of Biotechnology, Chemistry and Pharmacy, University of Siena, Siena 53100, Italy.

*Author for correspondence (cosima.baldari@unisi.it)

DOI: 10.1242/jcs.200006; E.P., 0000-0001-6881-9176; C.T.B., 0000-0002-4414-6744

Received 22 November 2016; Accepted 30 January 2017

required for the recycling of CXCR4, which is not regulated by IFT20 (Finetti et al., 2015; Onnis et al., 2015). These data suggest the existence of multiple specialized pathways that intersect by combining shared regulators to control recycling of specific receptors in T cells. Data obtained in a CD4 T-cell-specific conditional IFT20^{-/-} mouse have extended and validated *in vivo* the role of IFT20 in the assembly of a functional IS, implicating IFT20 also in the traffic of vesicular LAT (Vivar et al., 2016).

To further characterize the recycling pathway responsible for endosomal TCR trafficking to the IS, here, we used an unbiased approach to define novel IFT20 interactors by quantitative mass spectrometry (MS). We identified seven binding partners of IFT20, which included two interactors previously identified in T cells, i.e. IFT57 and IFT88 (Finetti et al., 2009, 2014), and five new interactors, namely IFT54 (also known as TRAF3IP1), GMAP-210 (also known as TRIP11), Arp2/3 complex subunit-3 (ARPC3), COP9 signalosome subunit-1 (CSN1, also known as GPS1) and ERGIC-53 (also known as LMAN1). Of these, three were found to be required for TCR trafficking to the IS.

RESULTS

Identification of novel IFT20 interactors by mass spectrometry

We undertook to identify IFT20-interacting partners by quantitative MS. A Tween StrepTagII was adjoined to the IFT20 C-terminus (IFT20-OST) to rapidly and quantitatively capture it and maximize recovery of protein partners. Total lysates of Jurkat T cells stably expressing IFT20-OST were subjected to pulldown using StrepTactin, eluted with biotin and analysed by nano-liquid chromatography tandem MS (nano-LC-MS/MS) (Fig. 1A).

StrepTactin pulldown in Jurkat cells not expressing IFT20-OST was used as a negative control. Data were analysed by label-free quantification using the MaxQuant software. Only proteins detected in none of three replicates in the negative control and that had a >2-fold abundance over control sample were considered as likely interactors.

Table 1 shows the potential IFT20-binding partners that passed these criteria, namely IFT54, IFT57, IFT88, GMAP-210, ARPC3, CSN1 and ERGIC-53. Of these, IFT57 and IFT88 have been previously reported to interact with IFT20 in T cells (Finetti et al., 2009), demonstrating the efficacy and specificity of our experimental procedure. ARPC3 is a component of Arp2/3 complex that is involved in F-actin nucleation and it is known to participate in IS assembly (Billadeau et al., 2007). IFT54 is part of the IFT-B complex, which includes IFT20, IFT57 and IFT88 and is required for ciliogenesis, but it has also been implicated in microtubule stability (Bizet et al., 2015; Berbari et al., 2011; Guo et al., 2010; Follit et al., 2009). The golgin GMAP-210 is a known IFT20 interactor in ciliated cells, where it has been shown to tether IFT20 to the Golgi (Follit et al., 2006; Follit et al., 2008). ERGIC-53 is an intermediate compartment protein mediating vesicle recycling from the endoplasmic reticulum (ER) to the Golgi (Zhang et al., 2009). The implication of ARPC3, IFT54 and GMAP-210 in intracellular trafficking and cytoskeleton organization is consistent with the role of IFT20 in regulating vesicular trafficking in T cells. The only traffic-unrelated IFT20 interactor identified in our analysis is CSN1, a component of the COP9 signalosome complex implicated in the ubiquitin–proteasome pathway, which suggests that IFT20 may participate in other cellular processes beyond its established function in vesicular traffic.

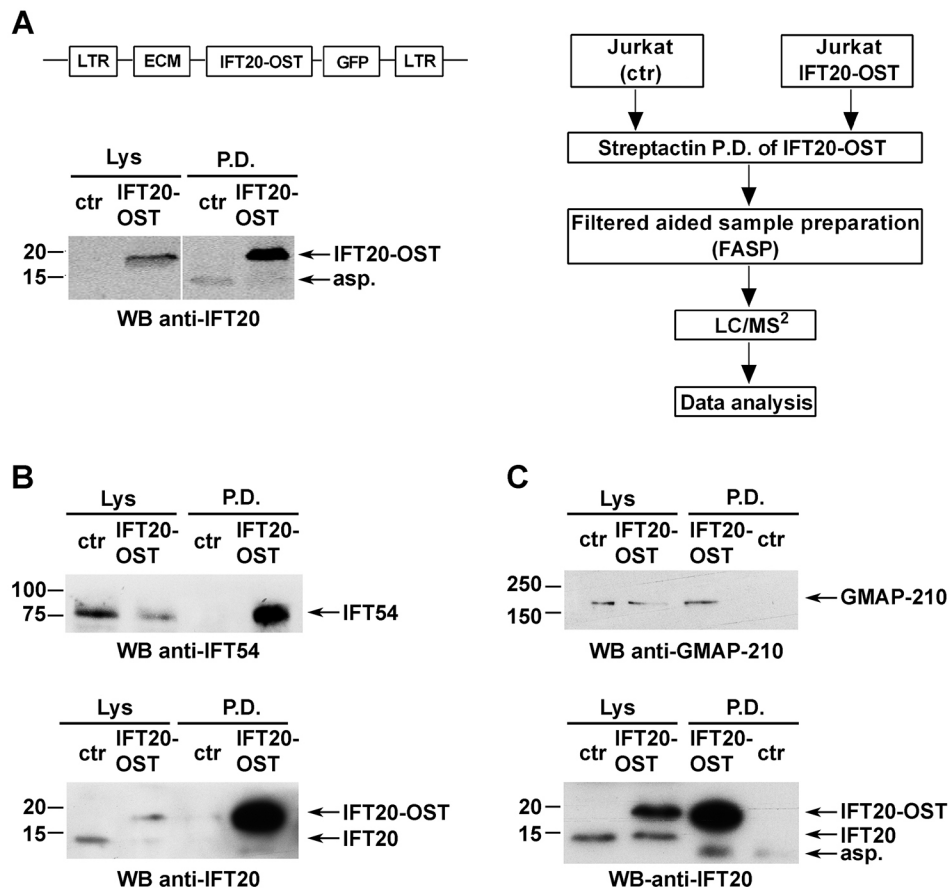


Fig. 1. IFT20 directly interacts with IFT54 and GMAP-210 in T cells. (A) Left panel, representative image of Streptactin pulldowns (P.D.) of IFT20-OST from lysates of resting untransduced Jurkat cells (negative control; ctr) and a stable Jurkat transfectant expressing IFT20-StrepTag (JIFT20-OST) ($n \geq 3$). Protein complexes isolated by Streptactin pulldown were processed for MS analysis as described in the experimental workflow (right panel). (B,C) Immunoblot analysis with anti-IFT54 or anti-GMAP-210 antibodies of IFT20-OST Streptactin pulldowns from lysates of resting control and JIFT20-OST cells. Input lysates (Lys) are shown. The immunoblots shown are representative of three independent experiments.

Table 1. IFT20 interactors identified by mass spectrometry

Accession no.	Protein name	Peptide sequences	IFT20 OST P.D. LFQ intensity	Neg. ctr P.D. LFQ intensity	Fold change	% sequence coverage	Andromeda score
Q8IY31 (IFT20_HUMAN)	Intraflagellar transport protein 20 homolog	5+4+6	49,949×10 ⁴	–	infinite	69.7	73.8
Q8TDR0 (MIPT3_HUMAN)	Intraflagellar transport protein 54 homolog	9+6+5	14,712×10 ⁴	–	infinite	22.2	625
Q15643 (TRIPB_HUMAN)	Golgi associated microtubule-binding protein 210	39+42+18	43,079×10 ⁴	–	infinite	37.3	317
Q9NWB7 (IFT57_HUMAN)	Intraflagellar transport protein 57 homolog	4+1+0	2803×10 ⁴	–	infinite	10.7	9.8
P49257 (LMAN1_HUMAN)	Protein ERGIC-53	3+2+0	631×10 ⁴	–	infinite	9.4	5.9
C9JFE4	COP9 signalosome complex subunit 1	2+2+0	275×10 ⁴	–	infinite	7.6	4.6
F5H6C2 (F5H6C2_HUMAN)	Intraflagellar transport protein 88 homolog	1+1+0	113×10 ⁴	–	infinite	69.7	4.07
O15145 (IFT20_HUMAN)	Actin-related protein 2/3 complex subunit 3	1+1+0	49,949×10 ⁴	–	infinite	69.7	3.7

Data were converted into .mzXML format using MSconvert (Proteowizard) and uploaded into the Central Proteomics Facility Pipeline (CPFP). Label-free quantification was performed using Maxquant software. Only proteins detected in none of the three replicates in the negative control (neg. ctr) and that had a >2-fold abundance over the control sample were considered as true interactors.

IFT20 directly interacts with IFT54 and GMAP-210

To independently validate the proteins identified by MS as IFT20 partners, we carried out an immunoblot analysis of StrepTactin-bound proteins. Proteins were pulled down from post-nuclear supernatants of control (ctr) and IFT20–OST-expressing Jurkat cells under the same conditions used for the MS analysis. Immunoblotting using antibodies specific for each interactor highlighted the presence of IFT54 (Fig. 1B) and GMAP-210 (Fig. 1C) in the IFT20–OST pull-down but not in the negative control, confirming a direct interaction of IFT20 with these two proteins. Of note, IFT54 was found to associate with β -tubulin in T cells, similar to in ciliated cells (Fig. S1). At variance with IFT54 and GMAP-210, ARPC3, CSN1 and ERGIC-53 were found both in IFT20–OST pulldown and in the negative control (data not shown), likely due to non-specific binding of the antibody to the StrepTactin beads, since MS analysis never detected these three proteins in the negative control sample.

The IFT20 interactors IFT54, ARPC3 and ERGIC-53 participate in IS assembly

Next, we investigated whether IFT54, ARPC3 and ERGIC-53, similarly to IFT20, were implicated in the regulation of vesicular traffic and IS assembly in T cells. Expression of each of these interactors was stably knocked down by short hairpin RNA interference (reduction of ~73% IFT54, ~74% GMAP-210, ~76% ARPC3, ~81% CSN1, ~85% ERGIC-53) (Fig. 2A). A transfectant generated with non-targeting short hairpin was used as control. Surface TCR–CD3 complex expression was comparable in all transfectants (Fig. S2A). To assess the role of the IFT20 partners in IS assembly, control and knocked down cells were incubated with Staphylococcal enterotoxin E (SEE)-pulsed Raji cells and subjected to a confocal imaging-based assay to detect TCR accumulation at the IS. Immunofluorescence analysis of the Jurkat T-cell conjugates with SEE-pulsed APCs using anti-CD3 antibody showed that the TCR–CD3 complexes failed to accumulate at the IS in a significant proportion of Jurkat cells knocked down for IFT54, ARPC3 or ERGIC-53, at variance with control cells (Fig. 2B). Conversely, no differences in the proportion of conjugates harbouring synaptic TCRs was observed in GMAP-210 KD or CSN1 KD cells (Fig. 2B), ruling out a role for these proteins in TCR recruitment

to the IS. Consistent with this defect, signalling was impaired in IFT54 knockdown (KD), ARPC3 KD or ERGIC-53 KD cells compared to control cells, as assessed by staining with anti-phosphotyrosine antibody, while conjugates formed between SEE-pulsed Raji cells and CSN1 KD or GMAP-210 KD cells showed a phosphotyrosine pattern comparable to that in control cells (Fig. 2C). The defect in TCR accumulation and phosphotyrosine signalling at the IS in cells depleted of IFT54, ARPC3 or ERGIC-53 was confirmed in primary T cells purified from healthy donors and infected with the respective shRNA-engineered lentiviral particles (Fig. 3). Collectively, these results indicate that, of the five new IFT20 interactors identified, IFT54, ARPC3 and ERGIC-53 are required for synaptic targeting of the TCR and downstream signalling, and suggest that these proteins cooperate with IFT20 in the assembly of a functional IS.

IFT54, ARPC3 and ERGIC-53 participate in IFT20-dependent TCR and Tfr recycling to the IS

Multiple mechanisms contribute to the transport of TCR complexes to the IS to sustain signalling for the extended timeframe required for T cell activation (Soares et al., 2013a). The implication of IFT20 in polarized TCR and Tfr recycling to the IS (Finetti et al., 2014, 2009) suggests that its interactors may participate in the trafficking pathway regulated by the IFT system in T cells. To address this issue, we first asked whether depletion of IFT54, ARPC3 or ERGIC-53 affects the translocation of the microtubule-organizing centre (MTOC) to the subsynaptic area, a process which is triggered by the TCR–CD3 complexes initially recruited to the IS from the plasma membrane-associated pool (Soares et al., 2013a). Conjugates formed by control Jurkat cells, or cells knocked down for IFT54, ARPC3 or ERGIC-53, with SEE-pulsed Raji cells were analysed by confocal microscopy using an anti- γ -tubulin antibody. No differences were found in the proportion of conjugates with a correct MTOC polarization between control and knockdown conjugates, indicating that IFT54, ARPC3 and ERGIC-53 are not required for MTOC translocation (Fig. 4). In support of this notion, the distance of the MTOC from the synaptic membrane in SEE-specific T-cell–APC conjugates was comparable between control T cells and cells depleted of IFT54, ARPC3 or ERGIC-53 (Fig. 4). Since this step is a prerequisite for polarized endosome

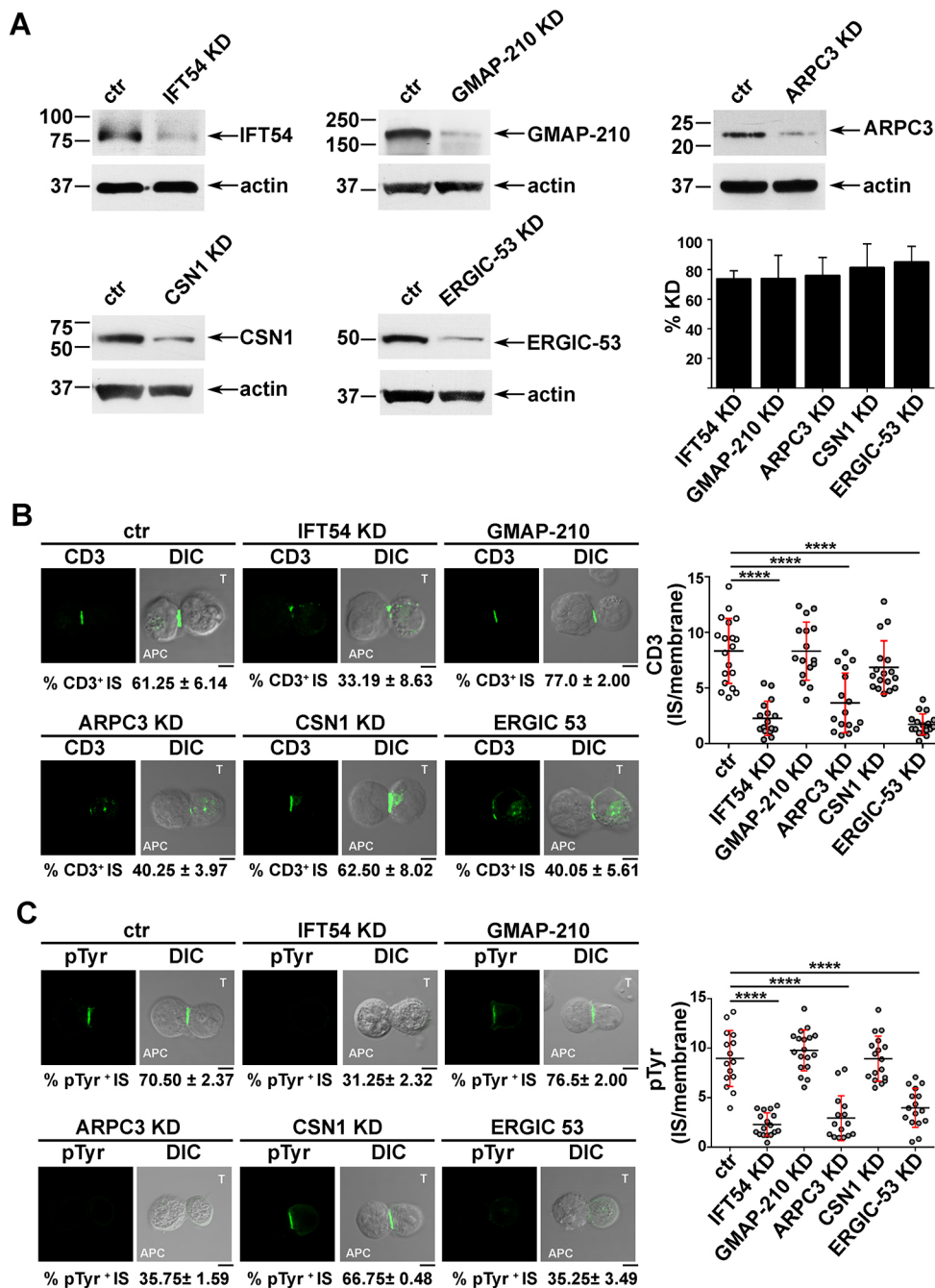


Fig. 2. The IFT20 interactors IFT54, ARPC3 and ERGIC53 participate in IS assembly. (A) Immunoblot analysis of IFT54, GMAP-210, ARPC3, CSN1 and ERGIC53 in lysates of Jurkat cells lentivirally transduced with non targeting control shRNA (ctr) or shRNA specific for each protein (KD). Representative immunoblot images are shown. The percentage knockdown of IFT54, GMAP210, ARPC3, CSN1 and ERGIC53 in the representative immunoblot was ~73%, ~74%, ~76%, ~81% and ~85%, respectively. The histogram on the right shows the mean±s.d. percentage of knockdown in each cell line ($n \geq 3$). (B,C) CD3 or pTyr immunofluorescence analysis in conjugates of SEE-pulsed Raji cells (APC) and Jurkat cells (labelled T) transduced with control shRNA or knocked down for IFT54, GMAP-210, ARPC3, CSN1 or ERGIC53. Median optical sections of representative conjugates are shown. Size bar: 5 μ m. The mean±s.d. of conjugates (%) showing CD3 or pTyr recruitment to the IS are indicated below the representative images. The graph on the right shows the ratio of CD3 or pTyr fluorescence intensity at the IS compared to the rest of the membrane as quantified with ImageJ. The red bars indicate the s.d. for each data set. At least 20 cells were analysed ($n \geq 3$). Measurements were taken on ≥ 250 conjugates ($n \geq 3$). **** $P < 0.0001$.

recycling to the IS, this result suggests that the defect in TCR accumulation at the IS might be caused by impaired traffic, similar to what occurs in IFT20 KD T cells (Finetti et al., 2009, 2014).

To address this issue, we tracked the fate of internalized TCRs in conjugates of IFT54 KD, ARPC3 KD or ERGIC-53 KD Jurkat T cells and SEE-pulsed APCs by confocal imaging. T cells were incubated with specific antibodies to induce TCR internalization. No differences in the rate and extent of TCR–CD3 internalization were observed among the different transfectants (Fig. S2B). Cells were acid-stripped to remove residual surface-bound monoclonal antibody (mAb) and then mixed with SEE-loaded Raji cells. Antigen-specific conjugates were stained with a fluorochrome-labelled secondary antibody without prior permeabilization. Under these conditions, we were only able to visualize the receptors that had been internalized and had recycled to the T-cell–APC contact

site (Finetti et al., 2014, 2015). The enrichment in TCR staining at the IS membrane was significantly reduced in IFT54 KD, ARPC3 KD or ERGIC-53 KD cells compared to in the control cells (Fig. 5A). A similar analysis was carried out for the Tfr. While surface Tfr levels and receptor internalization were comparable among the different transfectants (Fig. S2C,D), Tfr recycling to the IS was impaired in IFT54 KD, ARPC3 KD or ERGIC-53 KD cells, similar to recycling of the TCR (Fig. 6A). Hence IFT54, ARPC3 and ERGIC-53 are involved in the regulation of polarized TCR and Tfr recycling to the IS.

The involvement of IFT54, ARPC3 and ERGIC-53 in the targeting of TCR- and Tfr-positive recycling endosomes to the IS was further confirmed by staining conjugates with a fluorochrome-labelled secondary antibody after a fixation and permeabilization step. In this case, we were able to track mainly intracellular recycling

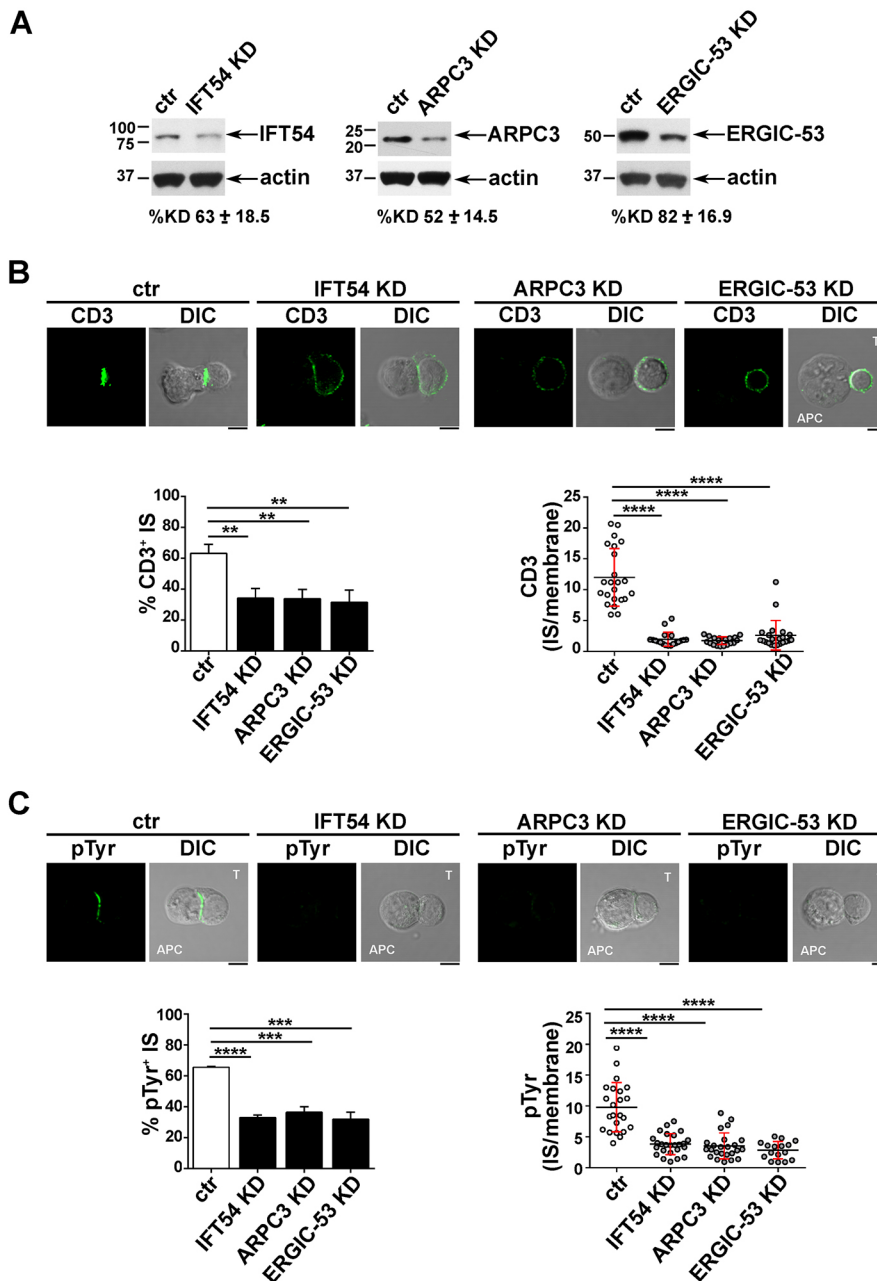


Fig. 3. The IFT20 interactors IFT54, ARPC3 and ERGIC53 participate in IS assembly in primary T cells. (A) Immunoblot analysis of IFT54, ARPC3 and ERGIC53 in lysates of primary T cells lentivirally transduced with non-targeting shRNA control (ctr) or shRNA specific for IFT54, ARPC3 or ERGIC-53 (KD). The immunoblot shown is representative of three independent experiments. Under each immunoblot, the mean±s.d. percentage knockdown obtained in the primary T cells isolated from three different healthy donors is indicated. (B,C) CD3 or pTyr immunofluorescence analysis in conjugates of primary T cells (labelled T) transduced as in A and Raji cells (APC), which were pulsed with a combination of three sAgs (SEE, SEB and SEA). Medial optical sections of representative conjugates are shown. The histogram on the left shows the mean±s.d. percentage of conjugates with TCR–CD3 accumulation (B) or pTyr staining (C), at the IS. Measurements were taken on ≥180 conjugates ($n \geq 3$). The graph on the right shows the ratio of CD3 or pTyr fluorescence intensity at the IS compared to the rest of the membrane quantified using ImageJ. The red bars indicate the s.d. for each data set. At least 25 cells were analysed ($n \geq 3$). Scale bars: 5 μ m. ** $P < 0.01$; *** $P < 0.001$; **** $P < 0.0001$.

endosomes containing TCRs or Tfr that had been internalized but had not yet undergone polarized recycling to the IS, as the membrane-associated TCRs were largely lost upon permeabilization. At variance with control antigen-specific conjugates, endosomes containing internalized TCR and Tfr failed to polarize toward the APC in the absence of IFT54, ARPC3 or ERGIC-53, and remained accumulated at the cell periphery (Figs 5B, 6B). Collectively, these results indicate that the IFT20 partners IFT54, ARPC3 and ERGIC-53 regulate polarized TCR and Tfr recycling to the IS, likely acting in concert with IFT20.

IFT54, ARPC3 and ERGIC-53 contribute to T cell activation

The finding that the IFT20-binding partners IFT54, ARPC3 and ERGIC-53 participate in polarized TCR and Tfr recycling, which is required for sustained signalling at the IS, suggests that they might contribute to T cell activation. To address to this question, we first carried out an immunoblot analysis for ERK1 and ERK2 (ERK1/2,

also known as MAPK3 and MAPK1, respectively) phosphorylation in response to CD3 and CD28 co-stimulation in a timecourse experiment. IFT54 deficiency was found to impair ERK1/2 phosphorylation at all time points, suggesting that this protein is required to both initiate and sustain TCR signalling (Fig. 7A, left panel). Similar results were obtained for ERGIC-53 (Fig. 7A, right panel). Conversely, a defect in ERK1/2 phosphorylation was observed only at later time points (10 min) in ARPC3 KD cells (Fig. 7A, central panel), indicating that the TCR-induced phosphorylation cascade was initiated normally but was not sustained in the absence of ARPC3.

As a complement to these experiments, we analysed the accumulation at the IS of active Zap70, a tyrosine kinase essential for the initiation of TCR signalling, by confocal microscopy (Wang et al., 2010). Consistent with a role for IFT54 and ERGIC-53 in promoting the targeting of recycling TCRs to the synaptic membrane to sustain signalling, the accumulation of phospho-

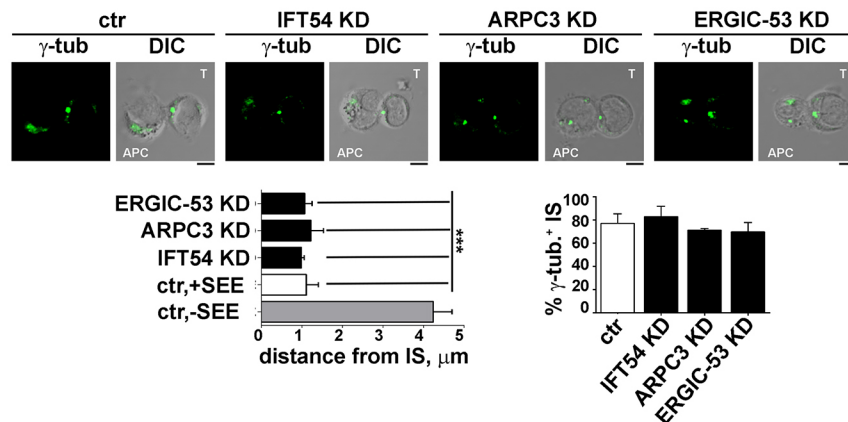


Fig. 4. IFT54, ARPC3 or ERGIC-53 deficiency does not affect MTOC polarization. Immunofluorescence analysis of γ -tubulin (centrosome marker) in conjugates of control (ctr) or IFT54, ARPC3 KD or ERGIC-53 KD T cells (labelled T) and SEE-pulsed Raji cells (APC). Medial optical sections of representative conjugates are shown. The quantification of MTOC distance from the T-cell–Raji-cell interface is shown below the images (left panel). Measurements were taken on 45 conjugates from three independent experiments (mean \pm s.d.). In the lower-right panel, the quantification (%) of conjugates harbouring subsynaptic γ -tubulin at the IS is shown. Measurements were taken on 180 conjugates from three independent experiments (mean \pm s.d.). Scale bars: 5 μ m. *** P <0.001.

Zap70 at the IS of Jurkat–Raji cell conjugates was impaired in the absence of these proteins (Fig. 7B). Conversely, ARPC3 deficiency did not affect phospho-Zap70 accumulation at the IS (Fig. 7B), indicating that ARPC3 participates in T-cell activation downstream of TCR-proximal signalling.

To investigate whether the IS defects observed in T cells depleted of IFT54, ARPC3 or ERGIC-53 translate in a modified biological outcome, we analysed the surface expression of the activation marker CD69 by flow cytometry. The deficiency of IFT54, as well as of either ARPC3 or ERGIC-53, resulted in a reduction in CD69 expression (Fig. 7C), confirming a role for these IFT20 interactors in T cell activation.

DISCUSSION

We have recently implicated IFT20, a component of the IFT system that is responsible for the assembly and maintenance of cilia and flagella, in the regulation of polarized TCR recycling to the IS. Moreover, we provided evidence for a crosstalk between IFT20 and the Rab-based machinery in the regulation of this process (Finetti et al., 2014, 2015; Onnis et al., 2015) and showed that IFT20 forms a complex with the IFT components IFT52, IFT57 and IFT88 (Finetti et al., 2009, 2014). Here, we show by quantitative MS analysis that IFT20 interacts with two interacting partners previously recognized in ciliated cells, namely IFT57 and IFT88, and identify IFT54, GMAP-210, ARPC3, CSN1 and ERGIC-53 as new IFT20-binding partners in T cells. None of these proteins showed any changes in the IFT20 interactome profile of anti-CD3-stimulated cells compared to resting cells (data not shown). Since four of the seven interactors share biological functions with IFT20, we considered them as bona fide IFT20 functional partners. IFT54 and GMAP-210 have been previously described as IFT20 interactors in ciliated cells (Follit et al., 2008, 2009; Bizet et al., 2015). This interaction was found to extend to T cells, as assessed by pulldown assays. Although the identification of genuine binding partners supports the robustness of the experimental approach, we were unable to validate the interaction of IFT20 with ARPC3, CSN1 and ERGIC-53 by immunoblot analysis despite the specific detection by MS over three replicates due to the presence of immunoreactive bands in the negative control pulldown sample (data not shown). It is noteworthy that, while three IFT proteins were found to be pulled down by IFT20 in the proteomic analysis, consistent with their participation in a multimolecular complex in ciliated cells (Follit et al., 2006, 2009; Taschner et al., 2016), no additional components of the complexes in which ARPC3 and CSN1 participate, i.e. Arp2/3 and the COP9 signalosome, respectively, were present among the IFT20 interactors. While we

cannot rule out that these complexes are labile and only some interactions are preserved under the lysis conditions used, it is possible that IFT20 may interact with individual subunits of the complexes to assist their assembly or alternatively to form new complexes with a different composition and function.

Interestingly, of the five new IFT20 interactors identified by MS in T cells, only three, namely IFT54, ARPC3 and ERGIC-53, participate in IS assembly, as assessed by the outcome of their depletion on synaptic TCR–CD3 accumulation and phosphotyrosine signalling in conjugates with SEE-loaded APCs, which leads to impaired T-cell activation. This results from their ability to regulate polarized recycling to the IS not only of the TCR, but also of the T β R, similar to IFT20 (Finetti et al., 2014), indicating that these proteins participate in the trafficking pathways controlled by IFT20.

Although IFT54 has long been known as a component of the IFT-B complex in the model organism *Chlamydomonas reinhardtii*, its role in IFT-dependent ciliogenesis in more complex organisms, including mammals, has only recently been reported (Li et al., 2008; Omori et al., 2008; Follit et al., 2009; Berbari et al., 2011). Human IFT54 was initially identified as a microtubule-binding protein (microtubule-interacting protein associated with TRAF3, MIPT3) implicated in the sequestration of TNFR-associated factor-3 and neuronal DISC1 to the cytoskeleton (Ling and Goeddel, 2000; Morris et al., 2003). A recent report identifying IFT54 mutations in patients affected by nephronophthisis (NPH), an autosomal-recessive nephropathy, further supports a role for IFT54 in the regulation of microtubule cytoskeleton dynamics. NPH-associated mutations were indeed found to increase the levels of microtubule-associated protein 4 (MAP4) and its binding to the cytoskeleton, which leads to microtubule hyperacetylation and enhanced microtubule stability (Bizet et al., 2015). This suggests a role for IFT54 as a negative regulator of microtubule stability beyond its role in ciliogenesis. Of note, the IFT-B complex components have been recently shown to be organized in two stable sub-complexes, IFT-B1 (core) and IFT-B2 (peripheral), in *Chlamydomonas reinhardtii*, with IFT54 participating in the IFT-B2 sub-complex and binding α - and β -tubulin dimers, which places IFT54 in an ideal position to bind tubulin and allow IFT movement along to the cilium (Taschner et al., 2016). Taken together with our results showing that IFT54 co-immunoprecipitates with β -tubulin in T cells, it is tempting to speculate that in the non-ciliated T cells IFT54 could promote the movement of recycling endosomes en route to the IS via its association with microtubules.

Similar to IFT20 and IFT54, the Arp2/3 complex component ARPC3 was also found to participate in the targeting of both TCR- and T β R-positive recycling endosomes to the T-cell–APC interface.

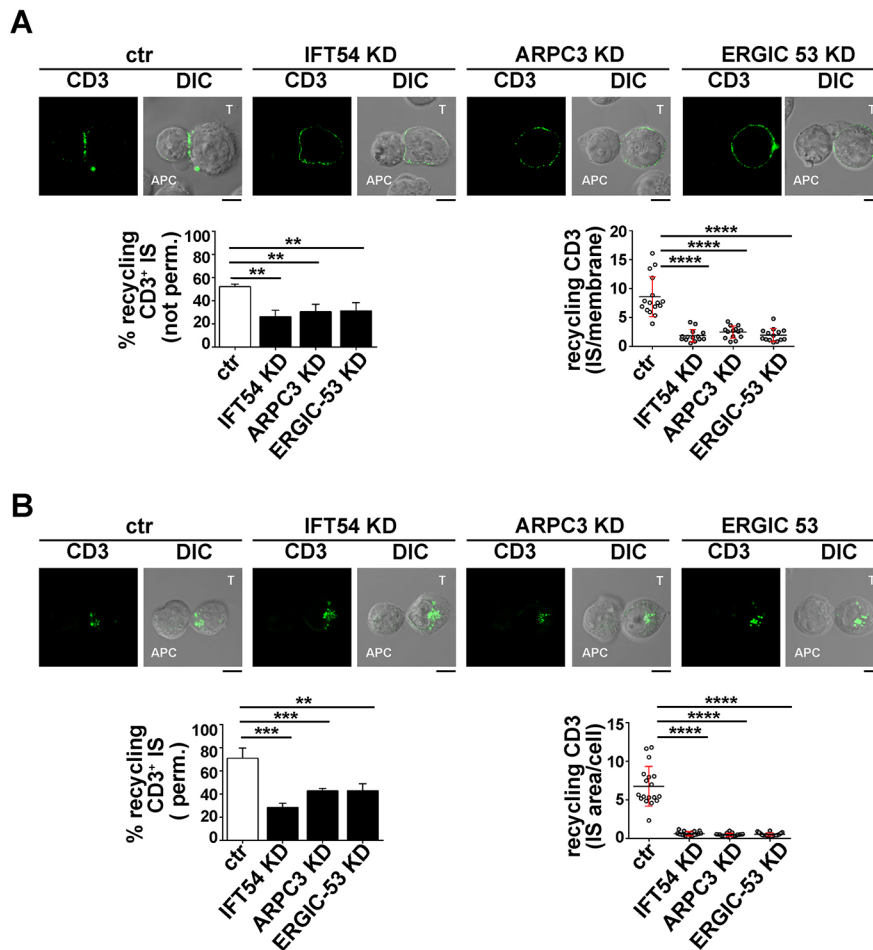


Fig. 5. IFT54, ARPC3 and ERGIC-53 participate in IFT20-dependent TCR recycling to the IS. (A) Immunofluorescence analysis under non-permeabilizing conditions of recycled TCRs (top) in conjugates of control (ctr) or IFT54 KD, ARPC3 KD or ERGIC-53 KD T cells (labelled T) and SEE-pulsed Raji cells (APC). Cells were incubated with saturating concentrations of receptor-specific mAbs at 37°C for 2 h. Residual surface-bound mAb was removed by acid stripping. Cells were then mixed with SEE-pulsed Raji cells and analysed under non-permeabilizing conditions, after paraformaldehyde fixation, by staining with fluorochrome-labelled secondary antibodies to track receptors that had been internalized and had recycled to the plasma membrane. Medial optical sections of representative conjugates are shown. The histogram on the lower-left shows the mean±s.d. percentage of conjugates harbouring recycled TCRs at the IS ($n \geq 3$). The graph on the lower-right shows the enrichment in recycling CD3 at the IS compared to the rest of the membrane, quantified using ImageJ. At least 20 cells were analysed ($n \geq 3$). (B) Immunofluorescence analysis, under permeabilizing conditions, of TCR-positive recycling endosomes in conjugates of control or IFT54 KD, ARPC3 KD or ERGIC-53 KD cells and SEE-pulsed Raji cells (APC). Cells were treated as described in B, but were fixed and permeabilized by immersion in methanol for 10 min at -20°C prior to imaging by confocal microscopy. Medial optical sections of representative conjugates are shown. The histogram on the lower-left shows the mean±s.d. percentage of conjugates harbouring polarization at the IS of endosomes carrying internalized TCRs undergoing recycling ($n \geq 3$). The graph on the lower-right shows the ratio of CD3 fluorescence intensity at the IS compared to the rest of the cell quantified using ImageJ. The red bars indicate the s.d. for each data set. At least 20 cells were analysed. Scale bars: 5 μm . ** $P < 0.01$; *** $P < 0.001$; **** $P < 0.0001$.

This result further supports a role for this actin-nucleating factor in the regulation of intracellular traffic to the IS in addition to its well-established function in actin cytoskeleton reorganization (Billadeau et al., 2007). Upon TCR engagement, the Arp2/3 complex nucleates new actin filaments following its association with the Wiskott–Aldrich syndrome protein superfamily nucleation-promoting factors, which include the endosome-associated member WASH (also known as WASH1) (Derivery et al., 2009). WASH participates in vesicle trafficking events by promoting Arp2/3-mediated F-actin polymerization on endosomes in cooperation with the retromer complex (Derivery et al., 2009; Gomez and Billadeau, 2009), is implicated in recycling of several receptors, including TCR, CD28, LFA-1, Tfr and GLUT1 (also known as SLC2A1) (Piotrowski et al., 2013), and has been found in endosomes polarizing to the IS in T cells (Gomez and Billadeau, 2009), similar to IFT20 (Finetti et al., 2014, 2009). Taken together with the ability of IFT20 to interact with

the TCR and Tfr in response to TCR engagement (Finetti et al., 2014), these results suggest that the interaction of IFT20 with ARPC3 may occur at endosomes carrying cargo tagged by IFT20 for polarized recycling to the IS. Of note, ARPC3 appears to function downstream of MTOC polarization, which is in agreement with a previous report by Gomez and colleagues showing that Arp 2/3 is dispensable for MTOC translocation which, by contrast, appears to be dependent on formin, another actin-nucleating factor (Gomez et al., 2007). Moreover, consistent with the report by Kumari et al. (2015), we found that distal TCR signalling is impaired in ARPC3-deficient cells, as assessed by the reduction of TCR-dependent ERK1/2 phosphorylation. Interestingly, the accumulation of active Zap70 at the IS was not affected by ARPC3 depletion, indicating that ARPC3 may be dispensable for TCR-proximal signalling but is required to sustain distal TCR signalling, including PLC- γ phosphorylation (Kumari et al., 2015). Consistent with this notion,

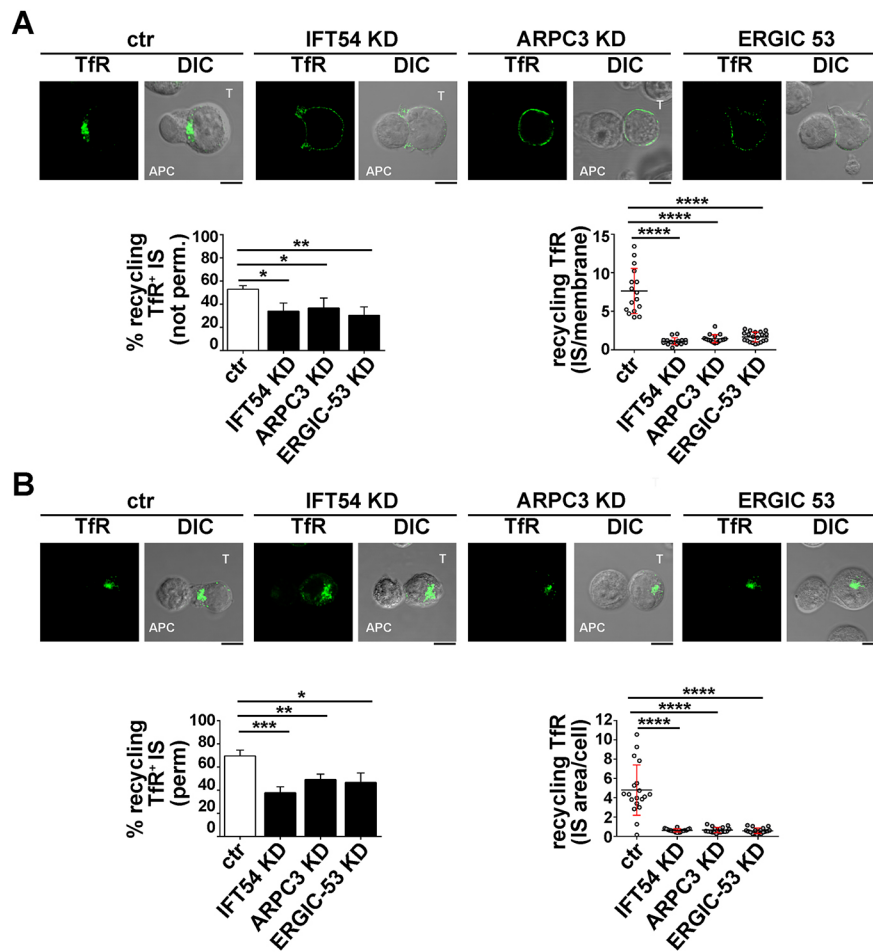


Fig. 6. IFT54, ARPC3 and ERGIC-53 participate in IFT20-dependent Tfr recycling to the IS. (A) Immunofluorescence analysis under non-permeabilizing conditions of recycled Tfr in conjugates of control or IFT54 KD, ARPC3 KD or ERGIC-53 KD T cells (labelled T) and SEE-pulsed Raji cells (APC). Cells were incubated with saturating concentrations of receptor-specific mAb at 37°C for 2 h. Residual surface-bound mAb was removed by acid stripping. Cells were then mixed with SEE-pulsed Raji and analysed under non-permeabilizing conditions, after paraformaldehyde fixation, by staining with fluorochrome-labelled secondary antibodies to track receptors that had been internalized and had recycled to the plasma membrane. Medial optical sections of representative conjugates are shown. DIC, differential interference contrast. The histogram on the left shows the mean percentage of conjugates harbouring recycled Tfrs at the IS ($n \geq 3$). The graph on the right shows the enrichment in recycling Tfrs at the IS compared to the rest of the membrane, as quantified using ImageJ. The red bars indicate the s.d. for each data set. At least 20 cells were analysed ($n \geq 3$). (B) Immunofluorescence analysis under permeabilizing conditions of Tfr-positive recycling endosomes in conjugates of control or IFT54 KD, ARPC3 KD or ERGIC-53 KD cells and SEE-pulsed Raji cells (APC). Cells were treated as described in A, but were fixed and permeabilized by immersion in methanol for 10 min at -20°C prior to imaging by confocal microscopy. Medial optical sections of representative conjugates are shown. The histogram on the left shows the mean percentage of conjugates harbouring polarization at the IS of endosomes carrying internalized Tfrs undergoing recycling ($n \geq 3$). The graph on the right shows the ratio of Tfr fluorescence intensity at the IS compared to the rest of the cells, as quantified using ImageJ. The red bars indicate the s.d. for each data set. At least 20 cells were analysed ($n \geq 3$). Scale bars: 5 μm . * $P < 0.05$; ** $P < 0.01$; *** $P < 0.001$; **** $P < 0.0001$.

Arp2/3 has been implicated together with WASP in the formation of actin foci at the T cell IS to sustain downstream TCR signalling (Kumari et al., 2015).

Interestingly, our data identified ERGIC-53 as a novel regulator of TCR and Tfr recycling to the IS and T cell activation. ERGIC-53 is a 53-kDa non-glycosylated type I transmembrane protein that mainly marks the ER-to-Golgi intermediate compartment (ERGIC) (Zhang et al., 2009). So far a limited number of ERGIC-53 cargoes have been identified, including factor V and factor VIII, which are critical cofactors for the coagulation cascade proteases factor Xa and factor IXa. Moreover, ERGIC-53 has been suggested to play a role in the polymerization and secretion of IgM in combination with ERp44, another ER-resident protein (Cortini and Sitia, 2010). The defects in both TCR and Tfr recycling in cells lacking ERGIC-53 suggest a novel role for this protein in the exocytic pathway downstream of ER-to-Golgi transport. How ERGIC-53 interfaces

with IFT20 to regulate polarized recycling remains to be established, although its implication in cargo sorting suggests that it could cooperate with IFT20 in TCR and Tfr sorting from early endosomes for their transit to recycling endosomes (Finetti et al., 2014). Whether ERGIC-53 can associate with early and/or recycling endosomes in T cells has not been established to date. Nevertheless, the finding that it is also associated with the cis-Golgi and even with the plasma membrane (Zhang et al., 2009) makes it a realistic hypothesis that will need to be tested.

Notwithstanding their ability to interact with IFT20, GMAP-210 and CSN1 appear to be dispensable for TCR accumulation and phosphotyrosine signalling at the IS, suggesting that these two IFT20 partners are not involved in the trafficking pathways that contribute to the assembly of a functional IS. In ciliated cells, GMAP-210 is a member of the Golgin family that interacts with IFT20 to anchor it to the Golgi, where IFT20 has been proposed to

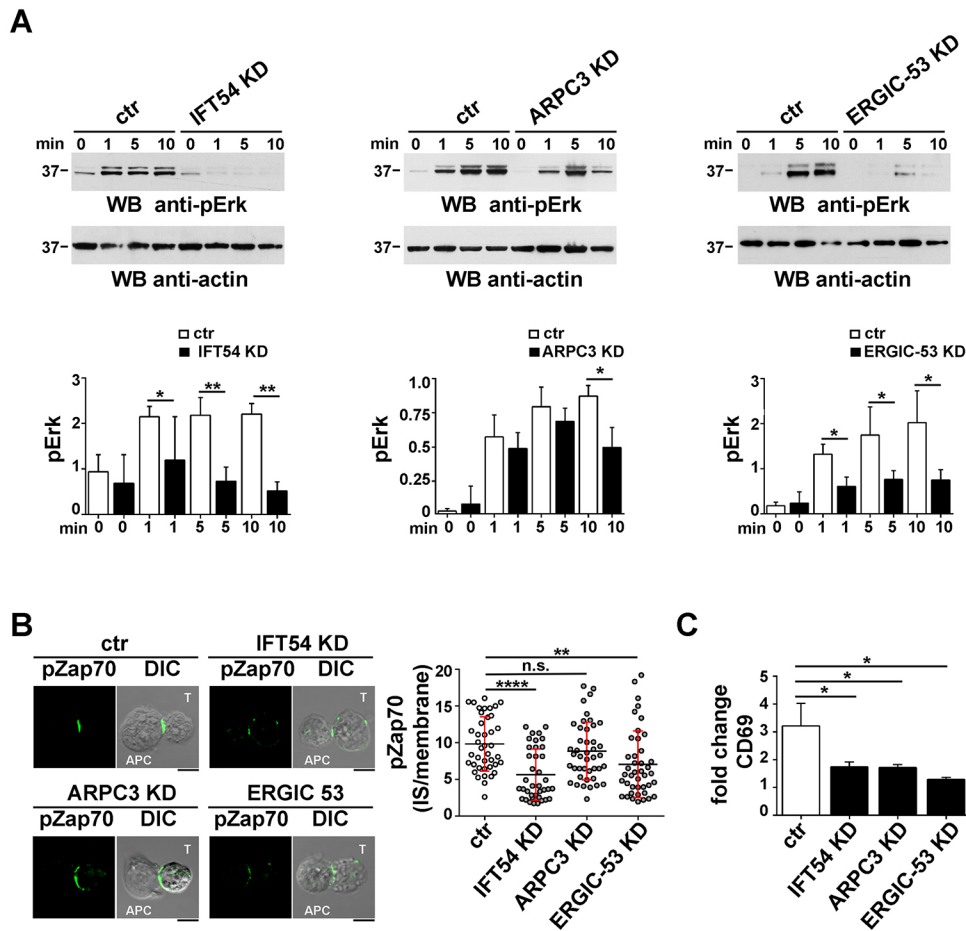


Fig. 7. IFT54, ARPC3 and ERGIC-53 contribute to T cell activation.

(A) Immunoblot analysis of ERK1/2 phosphorylation in control or IFT54 KD, ARPC3 KD or ERGIC-53 KD cells, either unstimulated or activated with anti-CD3 and anti-CD28 mAbs (1 μ g/ml) for the indicated times. The histogram shows the quantification of the 0, 1, 5 and 10 min time points. Data are normalized to the loading control and presented as mean \pm s.d. ($n \geq 3$). (B) Immunofluorescence analysis of pZap70 accumulation at the IS in conjugates of control or IFT54, ARPC3 KD or ERGIC-53 KD cells (labelled T) and SEE-pulsed Raji cells (APC). Conjugates were stained with a pZap70-specific (p-Y493) antibody. Medial optical sections are shown. Scale bars: 5 μ m. The graph shows the ratio of the pZap70 mean fluorescence intensity at the IS compared to the rest of the membrane, quantified using ImageJ. The horizontal red bars indicate the s.d. for each data set. Measurements were taken on 45 conjugates from three independent experiments. (C) Flow cytometric analysis of surface CD69 in control or IFT54 KD, ARPC3 KD or ERGIC-53 KD Jurkat cells incubated for 16 h with plate-bound anti-CD3 and anti-CD28 mAbs and then surface stained with an anti-CD69-FITC mAb and analysed by flow cytometry. The data refer to duplicate samples from three independent experiments. Error bars, s.d. * $P < 0.05$; ** $P < 0.01$; **** $P < 0.000$; ns, not significant.

sort proteins destined for the ciliary membrane (Follit et al., 2008). Interestingly, GMAP-210 mutant cells display defects in ciliary transport that are similar to those found in cells lacking IFT20 (Follit et al., 2008). While the IS has emerged as a homologue of the primary cilium in the non-ciliated T cell (Finetti and Baldari, 2013; Stinchcombe and Griffiths, 2014), our data indicate that GMAP-210 is dispensable for TCR traffic to the IS. We cannot, however, rule out at this stage the possibility that this protein is required for the sorting of other cargoes for delivery to the synaptic membrane.

Among the IFT20-binding partners identified in this study, CSN1 is the only protein that to date has not been linked to vesicular trafficking. CSN1 is the largest subunit of the COP9 signalosome, an evolutionarily conserved multimeric complex which in mammalian cells consists of eight subunits (CSN1 to CSN8) and acts as a negative regulator of the ubiquitin–proteasome degradation pathway (Wei and Deng, 2003). Of relevance, the COP9 signalosome subunits, CSN5 (also known as JAB1 or COPS5) and CSN8 (also known as COPS8), have been implicated in T cell homeostasis and development (Panattoni et al., 2008; Menon et al., 2007). Moreover, CSN5 promotes T cell activation through both the nuclear factor of activated T-cells (NF-AT) and NF- κ B pathways (Bianchi et al., 2000; Kinoshita et al., 2012; Welteke et al., 2009). Our results indicate that CSN1 does not cooperate with IFT20 in the regulation of TCR trafficking to the IS but do not rule out a role for this protein in signalling events downstream of TCR stimulation. Recent evidence has implicated the COP9 signalosome in another critical quality control pathway, namely, autophagy (Pearce et al., 2009; Su et al., 2011; Zhang et al., 2016). Remarkably, the IFT system has been shown to participate in the first steps of

autophagosome formation in ciliated cells (Pampliega et al., 2013). Our finding suggests the exciting possibility of an interplay between IFT20 and the COP9 signalosome in the regulation of T cell autophagy.

In summary, our results identify the IFT20 interactors IFT54, ARPC3 and ERGIC-53 as new players in the IFT20-dependent recycling pathway on which IS assembly and T-cell activation crucially depend. They also further underscore the role of the IFT20 in the regulation of vesicular pathways to the IS through its interaction with both other IFT proteins and trafficking-related proteins. Future experiments will help to better understand at which step of the IFT20-dependent recycling pathway IFT54, ARPC3 and ERGIC-53 are operational, as well as whether IFT20 could play other functions in T cells in combination with the other two interactors GMAP-210 and CSN1.

MATERIALS AND METHODS

Cells lines and plasmids

Stable cell lines include Jurkat 77 clone 20 T cells (a childhood T acute lymphoblastic leukemia cell line; Niedergan et al., 1995), Raji B cells (Burkitt's lymphoma cell line; Karpova et al., 2005) and human embryonic kidney epithelial cells (HEK) 293 cells, all of human origin (periodically tested for contamination). A Jurkat T cell line stably transfected with an OST-tagged IFT20 expression construct (pIFT20-OST) was also used. To generate the IFT20–OST expression construct, full-length cDNA encoding human IFT20 was isolated from total RNA extracted from Jurkat cells (NucleoSpin Rna, Machery-Nagel, Düren, Germany) and used as the PCR template to generate IFT20–OST, carrying a C-terminal Twin-StrepTag (IBA BioTAGnology, IBA GmbH, Goettingen, Germany) consisting of two Strep-tag (WSHPQFEK) moieties connected by a short linker

(WSHPQFEKggggggsggsaWSHPQFEK) (Schmidt et al., 2013). IFT20-OST was cloned into the lentiviral expression vector pHR-SIN-BX-IRES-Emerald kindly provided by Vincenzo Cerundolo (Weatherall Institute of Molecular Medicine, Oxford, UK), to generate lentiviral pHR-IFT20-OST, and verified by bidirectional sequencing. Stable knockdown cell lines were generated by lentiviral transduction of Jurkat cells and subsequent selection with 0.5 g/ml puromycin. To generate the stable knockdown Jurkat lines we used pLKO.1-puro non-target shRNA control lentiviral plasmid (ctr) and pLKO.1 shRNAs targeting IFT54 (TRCN000421123; IFT54 KD), GMAP-210 (TRCN00000220220; GMAP-210 KD), ARPC3 (TRCN000333116; ARPC3 KD), CSN1 (TRCN00036864; CSN1 KD) or ERGIC-53 (TRCN000433125; ERGIC-53 KD). pLKO.1-puro plasmids were from Sigma-Aldrich (Saint Louis, MO).

Lentiviral transduction in Jurkat T cells and primary human CD4⁺ T cells

HEK293T maintained in Dulbecco's modified Eagle's medium (DMEM; Sigma-Aldrich) and 10% fetal bovine serum (FBS; Thermo Scientific, Waltham, MA) were used as lentiviral packaging cells. Briefly, 2×10^6 cells were cultured overnight in a 10-cm tissue culture petri dish. The day after, cells were co-transfected with the pHR-IFT20-OST vector and the packaging plasmids psPAX2 and pMD2.G (provided by Didier Trono; Ecole Polytechnique Fédérale de Lausanne, Lausanne, Switzerland) by standard calcium phosphate precipitation. Medium was changed after 3 h. After 48 h at 37°C, viral supernatants were harvested, filtered (0.45 µm pore filters, Sarstedt, Nümbrecht, Germany) and used immediately for the transduction of Jurkat T cells in the presence of 5 µg/ml P-olybrene (Sigma-Aldrich) or snap-frozen in liquid nitrogen and stored at –80°C for future use. Peripheral blood samples were obtained from healthy donors after receiving their signed informed consent according to institutional guidelines. T cells were purified with the Human T-cell enrichment kit (STEMCELL Technologies, Vancouver, Canada) followed by Ficoll gradient centrifugation. Cells were incubated with human T-activator CD3–CD28 beads (Life Technologies-Thermo Scientific, Waltham, MA) at a beads-to-cell ratio of 1:5 in the presence of 50 U/ml IL-2 for 16 h prior to transduction. Cells were then harvested and resuspended in 800 µl RPMI (Sigma Aldrich). Then, 10% FBS was added with 200 µl concentrated lentiviral supernatant, 5 µg/ml polybrene and 50 U/ml IL-2. Cells were analysed 72 h post transduction.

Antibodies and reagents

IgG from OKT3 (anti-CD3ε) hybridoma supernatants were purified using Mabtrap (GE Healthcare, Milan, Italy) and titrated by flow cytometry. Anti-TfR monoclonal antibody (mAb; hybridoma OKT9) was generously provided by Andres Alcover (Pasteur Institute, Paris, France). All commercial antibodies used, with the respective source, catalogue number and dilution, are listed in Table S1. Staphylococcal enterotoxin E (SEE), Staphylococcal Enterotoxin B (SEB) and Staphylococcal Enterotoxin A (SEA) were from Toxin Technology (Sarasota, FL). Cell Tracker Blue was from Molecular Probes (Invitrogen); poly-L-lysine and protein-A–Sepharose was from GE Healthcare; Strep-Tactin–Sepharose beads were from IBA BioTAGnology.

Strep-Tactin–Sepharose pulldown assay

5×10^7 cells/sample of non-transduced Jurkat T cells (control) or of the IFT20-Streptag transfectant were lysed in ice-cold lysis buffer (20 mM Tris-HCl pH 7.5, 150 mM NaCl, 0.5% dodecyl-β-D-maltoside (Calbiochem-Merk Millipore) in presence of protease inhibitor mix (Calbiochem-Merk, Millipore) and Na_3VO_4 (Sigma Aldrich). Lysates were cleared by centrifugation at 14,000 g for 10 min 4°C. IFT20-OST pulldowns were carried out on cleared lysates for 30 min at 4°C with 125 µg Strep-Tactin–Sepharose (IBA BioTAGnology). After pulldown, beads were washed three times with lysis buffer, and bound proteins were eluted with 1× loading sample buffer (2.3% SDS, 0.0625 M Tris-HCl pH 6.8, 5% β-mercaptoethanol, 10% glycerol and 1% Bromophenol Blue) for western blotting analysis or with 25 mM biotin (Sigma Aldrich), 20 mM Tris-HCl pH 8.0 for 1 h at 4°C for MS analysis.

MS-based analysis

Samples were processed according to the filter-aided sample preparation (FASP) protocol (Wisniewski et al., 2009) using a 10 kDa molecular-mass cut-off Microcon filtration devices (Millipore cat. no MRCF0R030, Merck Millipore). Overnight digestion at room temperature was carried out using 300 µl of 12.5 ng/µl trypsin for each sample (Proteomics grade, Sigma-Aldrich) in 25 mM ammonium bicarbonate buffer. Peptide-rich eluates obtained from FASP digests were acidified to have 1% trifluoroacetic acid (TFA) (Reagent grade Sigma) and then desalted using a homemade C18 stage tip. Desalted peptides were eluted into autosampler vials using 70% acetonitrile, 0.1% formic acid and then lyophilized in a SpeedVac Concentrator 5301 (Eppendorf, Hamburg-Germany). Lyophilized peptides were re-suspended in 0.1% TFA and analysed by nanoLC-MS/MS using a QExactive (ThermoElectron, Hemel Hempstead, UK) mass spectrometer coupled to Dionex Ultimate 3000 RSLC nano HPLC system (ThermoElectron).

MS data analysis

Data were converted to .mgf file format using MSconvert (Proteowizard) and uploaded into the Central Proteomics Facility Pipeline (CPFP) for analysis (Trudgian et al., 2010). Enzyme was set to trypsin allowing for up to two missed cleavages. Carbamidomethyl cysteine was set as a fixed modification and oxidation (methionine), deamidation (NQ), acetylation (Protein-N) and phosphotyrosine as variable modifications. Mass tolerances for MS and MS/MS peak identifications were 20 ppm and 0.1 Da, respectively. InterProphet probability (IP Prob) is derived by the combination of results from multiple search engines within CPFP, and improves coverage and confidence over use of a single search engine. Label-free quantification was performed using MaxQuant software (Cox and Mann, 2008). The number of false-positive identifications was estimated from the percentage of decoy hits in the total protein list (false discovery rate, FDR). Proteins were filtered via the Contaminant Repository for Affinity Purification (CRAPOME) (Mellacheruvu et al., 2013). Only proteins detected in none of three replicates in the negative control and that were had a >2-fold abundance over the control sample were considered as true interactors.

Cell conjugate assay

For the IS experiments, Raji cells (used as APCs) were pulsed for 2 h with 10 µg/ml of the superantigens (sAg) SEE, SEB or SEA and labelled with 10 µM Cell Tracker Blue for the last 20 min. SEE was used for Jurkat T cells, which express a cognate TCR Vβ, whereas a combination of SEB, SEA and SEE was used for normal T cells, as these superantigens collectively cover a wider proportion of the Vβ repertoire compared to SEE. After sAg pulsing, APCs were washed, mixed with Jurkat cells (1:1) for 15 min and plated onto poly-L-lysine-coated wells of diagnostic microscope slides (Erie Microscope Slide- Thermo Scientific). Cells were allowed to adhere for 15 min and then fixed and permeabilized by immersion in methanol for 10 min at –20°C or by incubation in 4% paraformaldehyde in PBS for 20 min at room temperature and then permeabilized with 0.01% Triton X-100 in PBS. To study polarization at the T-cell–APC contact of TCR-positive endosomes or MTOC (γ-tubulin), or recruitment of tyrosine phosphoproteins (pTyr) or pZap70, fixed and permeabilized conjugates were stained with specific antibodies for 1 h at room temperature or overnight at 4°C. Cells were then rinsed and incubated with Alexa-Fluor-488-labelled secondary antibodies for 30 min at room temperature. Slides were washed in PBS and mounted in 90% glycerol and 10% PBS. Confocal microscopy was performed by using a Zeiss LSM700 (Carl Zeiss, Jena, Germany) microscope with a 63× objective. The z-series of optical sections were performed at 0.5-mm increments. Images were acquired with pinholes opened to obtain 0.8-mm-thick sections. Detectors were set to detect an optimal signal below the saturation limits.

Flow cytometric analysis of receptor internalization and T cell activation

Cells were incubated on ice with anti-CD3 or anti-TfR monoclonal to allow binding, washed to remove excess mAb (time 0) and shifted to 37°C for the indicated times (20, 60, 90, 120 min for CD3; 5, 10, 20, 30 min for TfR)

(Finetti et al., 2014). The relative levels of receptor were measured by labelling with fluorochrome-labelled secondary antibody both at time 0 (100%) and at each time point after the 37°C shift. Samples were analysed by flow cytometry. For *in vitro* T cell activation assays, Jurkat cells were incubated for 16 h with plate-bound anti-CD3 and anti-CD28 monoclonal antibodies for 16 h, surface stained with FITC-conjugated anti-CD69 monoclonal antibody for 1 h on ice and analysed by flow cytometry. Data were collected on a GUAVA Easy-Cyte 6-2 L flow cytometer (Merk Millipore) and analysed using FlowJo 6.0 software.

Confocal microscopy analysis of polarized receptor recycling to the IS

To measure recycling to the IS of TCR or Tfr internalized at the cell surface, cells were equilibrated for 30 min at 37°C in RPMI with 1% bovine serum albumin (BSA), then incubated with saturating concentrations of receptor-specific mAb for 2 h at 37°C. Residual surface-bound mAb was removed using an acid-stripping solution (30 s at room temperature in 100 mM glycine and 100 mM NaCl, pH 2.5). Cells were then mixed with Raji cells pulsed with SEE, SEB or SEA to form conjugates, incubated for 15 min at 37°C and plated onto poly-L-lysine-coated wells. Cells were fixed with 4% paraformaldehyde in PBS for 20 min and analysed under non-permeabilizing conditions. Alternatively, cells were fixed and permeabilized by immersion in methanol for 10 min at –20°C. Conjugates were stained with Alexa-Fluor-488-labelled secondary antibodies for 30 min to visualize internalized receptor–antibody complexes that had recycled to IS (non-permeabilized) or were still associated with recycling endosomes (permeabilized). Slides were washed in PBS and mounted in 90% glycerol with 10% PBS. Confocal microscopy was carried out as described above.

Image analysis

Images were analysed with ImageJ software (<https://imagej.nih.gov/ij/>). Briefly, the fluorescence intensity at the IS of CD3, pTyr, pZap70 or recycling CD3–Tfr (the latter two analysed under non-permeabilizing conditions) was divided by the mean of the average intensities measured in three regions of the same size at the plasma membrane outside of the IS (IS-to-membrane ratio). Alternatively, the fluorescence intensity of the recycling CD3- or Tfr-positive compartment accumulated at the IS in permeabilized conjugates was divided by the CD3 or Tfr fluorescence in the overall cell (IS area per cell).

Cell activation, immunoprecipitation and immunoblotting

Activation was performed by incubating Jurkat T cells (2×10^6) for the indicated times with anti-CD3 (1 µg/ml) and anti-CD28 (1 µg/ml) mAbs in RPMI. Cells were pelleted, washed twice in ice-cold PBS and lysed in 1% Triton X-100 in 20 mM Tris-HCl (pH 8) and 150 mM NaCl in the presence of protease inhibitors (Calbiochem-Merk Millipore) and 1 mM Na₃VO₄ (Sigma Aldrich). Lysates were cleared by centrifugation at 14,000 *g* for 10 min. For immunoprecipitation experiments, protein complexes were immunoprecipitated for 2 h using anti-IFT54 mAb and protein-A–Sephadex (3 mg/sample), after a pre-clearing step on protein-A–Sephadex (1 h, 3 mg/sample). Proteins were resolved by SDS-PAGE and transferred onto nitrocellulose membranes (0.45 µm Whatman, Protran, GE). Membranes were probed with the indicated antibodies followed by horseradish peroxidase (HRP)-conjugated secondary antibody. Labelled antibodies were detected using the enhanced chemiluminescence (ECL) kit (SuperSignal® WestPico Chemiluminiscent Substrate, Thermo Scientific). Membranes were re-probed with loading control antibody after stripping (Re-Blot Plus Western Blot Mild Antibody Stripping Solution, Merk Millipore). Blots were scanned using a laser densitometer (Duoscan T2500; Agfa, Milan, Italy) and quantified using ImageJ.

Statistical analysis

Mean values, standard deviation and *P*-values (unpaired non-parametric *t*-test) were determined using GraphPad Prism software (GraphPad Prism software, Inc., La Jolla, CA). The threshold for statistical significance was set to $P \leq 0.05$.

Acknowledgements

The authors wish to thank Benjamin Thomas and Svenja Hester for help with the mass spectrometry, André Cohnen for useful advice and Claire Hivroz for critical reading of the manuscript.

Competing interests

The authors declare no competing or financial interests.

Author contributions

D.G., A.O., O.A. and C.T.B. designed the experiments and analysed the data; D.G. and A.O. carried out the experiments; E.P. helped with mass spectrometry data analysis, F.G. provided key reagents and contributed to the lentiviral generation of stable Jurkat control and knockdown cell lines. D.G., O.A. and C.T.B. wrote the paper.

Funding

The financial support of Fondazione Telethon (grant no. GGP16003 to C.T.B.) and the Wellcome Trust (grant WT094296MA to O.A.) is gratefully acknowledged. Deposited in PMC for release after 6 months.

Supplementary information

Supplementary information available online at <http://jcs.biologists.org/lookup/doi/10.1242/jcs.200006.supplemental>

References

- Acuto, O., Di Bartolo, V. and Michel, F. (2008). Tailoring T-cell receptor signals by proximal negative feedback mechanisms. *Nat. Rev. Immunol.* **8**, 699–712.
- Bianchi, E., Denti, S., Granata, A., Bossi, G., Geginat, J., Villa, A., Rogge, L. and Pardi, R. (2000). Integrin LFA-1 interacts with the transcriptional co-activator JAB1 to modulate AP-1 activity. *Nature* **404**, 617–621.
- Berbari, N. F., Kin, N. W., Sharma, N., Michaud, E. J., Kesterson, R. A. and Yoder, B. K. (2011). Mutations in Traf3ip1 reveal defects in ciliogenesis, embryonic development, and altered cell size regulation. *Dev. Biol.* **360**, 66–76.
- Billadeau, D. D., Nolz, J. C. and Gomez, T. S. (2007). Regulation of T-cell activation by the cytoskeleton. *Nat. Rev. Immunol.* **7**, 131–143.
- Bizet, A. A., Becker-Heck, A., Ryan, R., Weber, K., Filhol, E., Krug, P., Halbritter, J., Delous, M., Lasbennes, M.-C., Linghu, B. et al. (2015). Mutations in TRAF3IP1/IFT54 reveal a new role for IFT proteins in microtubule stabilization. *Nat. Commun.* **6**, 8666.
- Bonello, G., Blanchard, N., Montoya, M. C., Aguado, E., Langlet, C., He, H.-T., Nunez-Cruz, S., Malissen, M., Sanchez-Madrid, F., Olive, D. et al. (2004). Dynamic recruitment of the adaptor protein LAT: LAT exists in two distinct intracellular pools and controls its own recruitment. *J. Cell Sci.* **117**, 1009–1016.
- Cortini, M. and Sitia, R. (2010). ERp44 and ERGIC-53 synergize in coupling efficiency and fidelity of IgM polymerization and secretion. *Traffic* **11**, 651–659.
- Cox, J. and Mann, M. (2008). MaxQuant enables high peptide identification rates, individualized p.p.b.-range mass accuracies and proteome-wide protein quantification. *Nature Biotechnol.* **26**, 1367–1372.
- Das, V., Nal, B., Dujancourt, A., Thoulouze, M.-I., Galli, T., Roux, P., Dautry-Varsat, A. and Alcover, A. (2004). Activation-induced polarized recycling targets T cell antigen receptors to the immunological synapse. *Immunity* **20**, 577–588.
- Derivery, E., Sousa, C., Gautier, J. J., Lombard, B., Loew, D. and Gautreau, A. (2009). The Arp2/3 activator WASH controls the fission of endosomes through a large multiprotein complex. *Dev. Cell* **17**, 712–723.
- Egen, J. G. and Allison, J. P. (2002). Cytotoxic T lymphocyte antigen-4 accumulation in the immunological synapse is regulated by TCR signal strength. *Immunity* **16**, 23–35.
- Ehrlich, L. I. R., Ebert, P. J. R., Krummel, M. F., Weiss, A. and Davis, M. M. (2002). Dynamics of p56lck translocation to the T cell immunological synapse following agonist and antagonist stimulation. *Immunity* **17**, 809–822.
- Finetti, F. and Baldari, C. T. (2013). Compartmentalization of signaling by vesicular trafficking: a shared building design for the immune synapse and the primary cilium. *Immunol. Rev.* **251**, 97–112.
- Finetti, F., Paccani, S. R., Riparbelli, M. G., Giacomello, E., Perinetti, G., Pazour, G. J., Rosenbaum, J. L. and Baldari, C. T. (2009). Intraflagellar transport is required for polarized recycling of the TCR/CD3 complex to the immune synapse. *Nat. Cell Biol.* **11**, 1332–1339.
- Finetti, F., Patrucci, L., Masi, G., Onnis, A., Galgano, D., Lucherini, O. M., Pazour, G. J. and Baldari, C. T. (2014). Specific recycling receptors are targeted to the immune synapse by the intraflagellar transport system. *J. Cell Sci.* **127**, 1924–1937.
- Finetti, F., Laura Patrucci, L., Galgano, D., Cassioli, C., Perinetti, G., Pazour, G. L. and Baldari, C. T. (2015). The small GTPase Rab8 interacts with VAMP-3 to regulate the delivery of recycling TCRs to the immune synapse. *J. Cell. Sci.* **128**, 2541–2552.

- Follit, J. A., Tuft, R. A., Fogarty, K. E. and Pazour, G. J. (2006). The intraflagellar transport protein IFT20 is associated with the Golgi complex and is required for cilia assembly. *Mol. Biol. Cell* **17**, 3781–3792.
- Follit, J. A., San Agustín, T. J., Xu, F., Jonassen, J. A., Samtani, R., Lo, C. W. and Pazour, G. J. (2008). The Golgin GMAP210/TRIP11 anchors IFT20 to the Golgi complex. *PLoS Genet.* **4**, 1–14.
- Follit, J. A., Xu, F., Keady, B. T. and Pazour, G. J. (2009). Characterization of mouse IFT complex B. *Cell. Motil. Cytoskeleton* **66**, 457–468.
- Fooksman, D. R., Vardhana, S., Vasiliver-Shamis, G., Liese, J., Blair, D. A., Waite, J., Sacristán, C., Vitorica, G. D., Zanin-Zhorov, A. and Dustin, M. L. (2010). Functional anatomy of T cell activation and synapse formation. *Annu. Rev. Immunol.* **28**, 79–105.
- Gomez, T. S. and Billadeau, D. D. (2009). A FAM21-containing WASH complex regulates retromer-dependent sorting. *Dev. Cell* **17**, 699–711.
- Gomez, T. S., Kumar, K., Medeiros, R. B., Shimizu, Y., Leibson, P. J. and Billadeau, D. D. (2007). Formins regulate the actin-related protein 2/3 complex-independent polarization of the centrosome to the immunological synapse. *Immunity* **26**, 177–190.
- Guo, C.-W., Xiong, S., Liu, G., Wang, Y.-F., He, Q.-Y., Zhang, X.-E., Zhang, Z.-P., Ge, F. and Kitazato, K. (2010). Proteomic analysis reveals novel binding partners of MIP-T3 in human cells. *Proteomics* **10**, 2337–2347.
- Karpova, M. B., Schoumans, J., Ernberg, I., Henter, J. I., Nordenskjöld, M. and Fadeel, B. (2005). Raji revisited: cytogenetics of the original Burkitt's lymphoma cell line. *Leukemia* **19**, 159–161.
- Kinoshita, S. M., Krutzik, P. O. and Nolan, G. P. (2012). COP9 signalosome component JAB1/CSN5 is necessary for T cell signaling through LFA-1 and HIV-1 replication. *PLoS ONE* **7**, e41725.
- Kumari, S., Curado, S., Mayya, V. and Dustin, M. L. (2014). T cell antigen receptor activation and actin cytoskeleton remodeling. *Biochim. Biophys. Acta* **1838**, 546–556.
- Kumari, S., Depoil, D., Martinelli, R., Judokusumo, E., Carmona, G., Gertler, F. B., Kam, L. C., Carman, C. V., Burkhardt, J. K., Irvine, D. J. et al. (2015). Actin foci facilitate activation of the phospholipase C- γ in primary T lymphocytes via the WASP pathway. *Elife* **4**, e04953.
- Larghi, P., Williamson, D. J., Carpiér, J.-M., Dogniaux, S., Chemin, K., Bohineust, A., Danglot, L., Gaus, K., Galli, T. and Hivroz, C. (2013). VAMP7 controls T cell activation by regulating the recruitment and phosphorylation of vesicular Lat at TCR-activation sites. *Nat. Immunol.* **14**, 723–731.
- Ley, S. C., Marsh, M., Bebbington, C. R., Proudfoot, K. and Jordan, P. (1994). Distinct intracellular localization of Lck and Fyn protein tyrosine kinases in human T lymphocytes. *J. Cell Biol.* **125**, 639–649.
- Li, C., Inglis, P. N., Leitch, C. C., Efimenko, E., Zaghoul, N. A., Mok, C. A., Davis, E. E., Bialas, N. J., Healey, M. P., Héon, E. et al. (2008). An essential role for DYF-11/MIP-T3 in assembling functional intraflagellar transport complexes. *PLoS Genet.* **4**, e1000044.
- Lillemeier, B. F., Mörtelmaier, M. A., Forstner, M. B., Huppa, J. B., Groves, J. T. and Davis, M. M. (2010). TCR and Lat are expressed on separate protein islands on T cell membranes and concatenate during activation. *Nat. Immunol.* **11**, 90–96.
- Ling, L. and Goeddel, D. V. (2000). MIP-T3, a novel protein linking tumor necrosis factor receptor-associated factor 3 to the microtubule network. *J. Biol. Chem.* **275**, 23852–23860.
- Mellacheruvu, D., Wright, Z., Couzens, A. L., Lambert, J.-P., St-Denis, N. A., Li, T., Miteva, Y. V., Hauri, S., Sardi, M. E. and Low, T. Y. (2013). The CRAPome: a contaminant repository for affinity purification–mass spectrometry data. *Nat. Methods* **10**, 730–736.
- Menon, S., Chi, H., Zhang, H., Deng, X. W., Flavell, R. and Wei, N. (2007). COP9 signalosome subunit 8 is essential for peripheral T cell homeostasis and antigen receptor-induced entry into the cell cycle from quiescence. *Nat. Immunol.* **8**, 1236–1245.
- Morris, J. A., Kandpal, G., Ma, L. and Austin, C. P. (2003). DISC1 (Disrupted-In-Schizophrenia 1) is a centrosome-associated protein that interacts with MAP1A, MIPT3, ATF4/5 and NUDEL: Regulation and loss of interaction with mutation. *Hum. Mol. Gen.* **12**, 1591–1608.
- Nachury, M. V., Seeley, E. S. and Jin, H. (2011). Trafficking to the ciliary membrane: how to get across the periciliary diffusion barrier? *Annu. Rev. Cell Dev. Biol.* **26**, 59–87.
- Niedergang, F., Hémar, A., Hewitt, C. R. A., Owen, M. J., Dautry-Varsat, A. and Alcover, A. (1995). The Staphylococcus aureus enterotoxin B superantigen induces specific T cell receptor down-regulation by increasing its internalization. *J. Biol. Chem.* **270**, 12839–12845.
- Omori, Y., Zhao, C., Saras, A., Mukhopadhyay, S., Kim, W., Furukawa, T., Sengupta, P., Veraksa, A. and Malicki, J. (2008). Elipsa is an early determinant of ciliogenesis that links the IFT particle to membrane-associated small GTPase Rab8. *Nat. Cell Biol.* **10**, 437–444.
- Onnis, A., Finetti, F., Patrussi, L., Gottardo, M., Cassioli, C., Spanò, S. and Baldari, C. T. (2015). The small GTPase Rab29 is a common regulator of immune synapse assembly and ciliogenesis. *Cell Death Differ.* **22**, 1687–1699.
- Pampliega, O., Orhon, I., Patel, B., Sridhar, S., Díaz-Carretero, A., Beau, I., Codogno, P., Satir, B. H., Satir, P. and Cuervo, A. M. (2013). Functional interaction between autophagy and ciliogenesis. *Nature* **502**, 194–200.
- Panattoni, M., Sanvito, F., Basso, V., Doglioni, C., Casorati, G., Montini, E., Bender, J. R., Mondino, A. and Pardi, R. (2008). Targeted inactivation of the COP9 signalosome impairs multiple stages of T cell development. *J. Exp. Med.* **205**, 465–477.
- Pearce, C., Hayden, R. E., Bunce, C. M. and Khanim, F. L. (2009). Analysis of the role of COP9 Signalosome (CSN) subunits in K562; the first link between CSN and autophagy. *BMC Cell Biol.* **28**, 10–31.
- Piotrowski, J. T., Gomez, T. S., Schoon, R. A., Mangalam, A. K. and Billadeau, D. D. (2013). WASH knockout T cells demonstrate defective receptor trafficking, proliferation, and effector function. *Mol. Cell Biol.* **33**, 958–973.
- Rosy, J., Owen, D. M., Williamson, D. J., Yang, Z. and Gaus, K. (2013). Conformational states of the kinase Lck regulate clustering in early T cell signaling. *Nat. Immunol.* **14**, 82–89.
- Sherman, E., Barr, V., Manley, S., Patterson, G., Balagopalan, L., Akpan, I., Regan, C. K., Merrill, R. K., Sommers, C. L., Lippincott-Schwartz, J. et al. (2011). Functional nanoscale organization of signaling molecules downstream of the T cell antigen receptor. *Immunity* **35**, 705–720.
- Schmidt, T. G. M., Batz, L., Bonet, L., Carl, U., Holzapfel, G., Kiem, K., Matulewicz, K., Niermeier, D., Schuchardt, I. and Stanar, K. (2013). Development of the Twin-Strep-tag[®] and its application for purification of recombinant proteins from cell culture supernatants. *Protein Expr. Purif.* **92**, 54–61.
- Soares, H., Lasserre, R. and Alcover, A. (2013a). Orchestrating cytoskeleton and intracellular vesicle traffic to build functional immunological synapses. *Immunol. Rev.* **256**, 118–132.
- Soares, H., Henriques, R., Sachse, M., Ventimiglia, L., Alonso, M. A., Zimmer, C., Thoulouze, M.-I. and Alcover, A. (2013b). Regulated vesicle fusion generates signaling nanoterritories that control T cell activation at the immunological synapse. *J. Exp. Med.* **210**, 2415–2433.
- Spanò, S., Liu, X. and Galán, J. E. (2011). Proteolytic targeting of Rab29 by an effector protein distinguishes the intracellular compartments of human-adapted and broad-host Salmonella. *Proc. Natl. Acad. Sci. USA* **108**, 18418–18423.
- Stinchcombe, J. C. and Griffiths, G. M. (2014). Communication, the centrosome and the immunological synapse. *Philos. Trans. R. Soc. Lond. B Biol. Sci.* **369**, 20130463.
- Su, H., Li, F., Ranek, M. J., Wei, N. and Wang, X. (2011). COP9 signalosome regulates autophagosome maturation. *Circulation* **124**, 2117–2128.
- Taschner, M., Weber, K., Mourão, A., Vetter, M., Awasthi, M., Stiegler, M., Bhogaraju, S. and Lorentzen, E. (2016). Intraflagellar transport proteins 172, 80, 57, 54, 38, and 20 form a stable tubulin-binding IFT-B2 complex. *EMBO J.* **35**, 773–790.
- Trudigian, D. C., Thomas, B., McGowan, S. J., Kessler, B. M., Salek, M. and Acuto, O. (2010). CPFP: a central proteomics facilities pipeline. *Bioinformatics* **26**, 1131–1132.
- Vivar, O., Masi, G., Carpiér, J. M., Magalhaes, J., Galgano, D., Pazour, G. J., Amigorena, S., Hivroz, C. and Baldari, C. T. (2016). IFT20 controls LAT recruitment to the immune synapse and T cell activation *in vivo*. *Proc. Natl. Acad. Sci. USA* **113**, 386–391.
- Wang, H., Kadlec, T. A., Au-Yeung, B. B., Goodfellow, H. E., Hsu, L. Y., Freedman, T. S. and Weiss, A. (2010). ZAP-70: An essential kinase in T-cell signaling. *Cold Spring Harb. Perspect. Biol.* **2**, a002279.
- Wei, N. and Deng, X. W. (2003). The COP9 signalosome. *Annu. Rev. Cell Dev. Biol.* **19**, 261–286.
- Welteke, V., Eitelhuber, A., Düwel, M., Schweitzer, K., Naumann, M. and Krappmann, D. (2009). COP9 signalosome controls the Carma1-Bcl10-Malt1 complex upon T-cell stimulation. *EMBO Rep.* **10**, 642–648.
- Williamson, D. J., Owen, D. M., Rosy, J., Magenau, A., Wehrmann, M., Gooding, J. J. and Gaus, K. (2011). Pre-existing clusters of the adaptor Lat do not participate in early T cell signaling events. *Nat. Immunol.* **12**, 655–662.
- Wiśniewski, J. R., Zougman, A., Nagaraj, N., Mann, M. and Wisniewski, J. R. (2009). Universal sample preparation method for proteome analysis. *Nat. Methods* **6**(5), 359–362.
- Yokosuka, T., Kobayashi, W., Sakata-Sogawa, K., Takamatsu, M., Hashimoto-Tane, A., Dustin, M. L., Tokunaga, M. and Saito, T. (2008). Spatiotemporal regulation of T cell costimulation by TCR-CD28 microclusters and protein kinase C θ translocation. *Immunity* **29**(4), 589–601.
- Zhang, Y. C., Zhou, Y., Yang, C. Z. and Xiong, D. S. (2009). A review of ERGIC-53: Its structure, functions, regulation and relations with diseases. *Histol. Histopathol.* **24**, 1193–1204.
- Zhang, Q. Y., Jin, R., Zhang, X., Sheng, J.-P., Yu, F., Tan, R.-X., Pan, Y., Huang, J.-J. and Kong, L.-D. (2016). The putative oncotarget CSN5 controls a transcription-uncorrelated p53-mediated autophagy implicated in cancer cell survival under curcumin treatment. *Oncotarget* **7**, 69688–69702.

Supplementary material

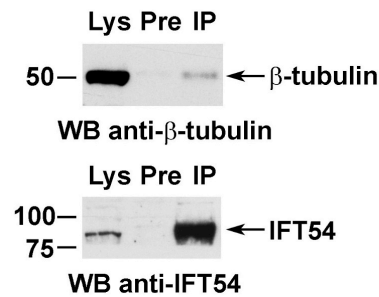


Figure S1. Immunoblot analysis of β -tubulin and IFT54 of IFT54-specific immunoprecipitate (IP) from lysates of resting Jurkat cells. Preclearing controls are included in each blot (neg. ctr). Total cell lysates were included in each gel to identify the migration of the proteins tested. The immunoblot shown is representative of 3 independent experiments.

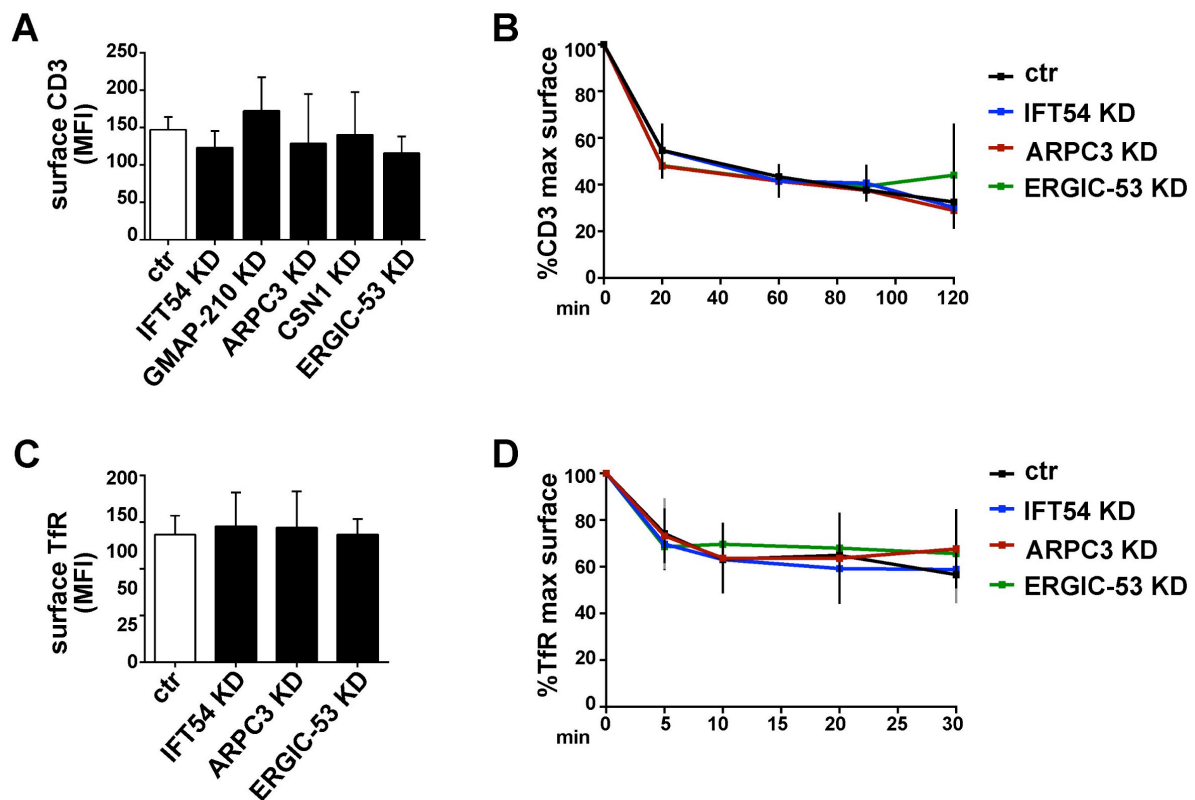


Figure S2. A. Jurkat cells lentivirally transduced with non-targeting control shRNA or shRNAs specific for IFT54 (~73% knock-down), GMAP-210 (~74% knock-down), ARPC3 (~76 % knock-down), CSN1 (~81% knock-down), or ERGIC-53 (~85% knock-down) were stained on ice with anti-CD3-PE and basal TCR surface expression was analyzed by flow cytometry. The data refer to duplicates from 3 independent experiments. Error Bars, SD **B.** Flow cytometric analysis of TCR internalization in control or IFT54 KD, ARPC3 KD or ERGIC-53 KD cells. Cells were incubated on ice with anti-CD3 mAb to allow binding, washed to remove excess mAb (time 0) and shifted to 37°C for the indicated times. The relative levels of receptor were measured by labelling with fluorochrome-labeled secondary antibody both at time 0 (100%) and at each time point after the 37°C shift. The data for each time point refer to duplicate samples from 3 independent experiments. Error bars, SD **C.** Basal TfR surface expression in control or IFT54 KD, ARPC3KD or ERGIC-53KD Jurkat cells assessed by flow cytometry, using anti-TfR mAb, followed by fluorochrome-labelled secondary Ab staining. The data for each time point refer to duplicate samples from 3 independent experiments. Error bars, SD. **D.** Flow cytometric analysis of TfR internalization in control or IFT54 KD, ARPC3 KD or ERGIC-53 KD Jurkat cells. Cells were incubated on ice with anti-TfR mAb to allow binding, washed to remove excess mAb (time 0) and shifted to 37°C for the indicated times. The relative levels of receptor were measured by labelling with fluorochrome-labelled secondary antibody both at time 0 (100%) and at each time point after the 37°C shift. The data for each time point refer to duplicate samples from 3 independent experiments. Error bars, SD.

Table S1. Commercial antibodies

Antibody	Host Species	Catalogue no	Source	Working dilution	Application
Anti-actin	mouse	MAB1501	Merk Millipore	1:2000	WB
Anti-ARPC3	rabbit	Sc-68396	Santa Cruz	1:1000	WB
Anti-CSN1	rabbit	11709-1-AP	ProteinTech	1:100	WB
Anti-IFT54	rabbit	14404-1-AP	ProteinTech	1:1000 1:200	WB IP
Anti-IFT20	rabbit	13615-1-AP	ProteinTech	1:1000	WB
Anti-ERGIC-53	mouse	Ab118407	AbCam	1:1000	WB
Anti-GMAP-210	mouse	611712	Becton Dickinson	1:250	WB
Anti-phosphorylated p44/42 (MAPK) Erk1/2	rabbit	9101	Cell Signaling	1:1000	WB
Anti-rabbit HRP	donkey	NA934	GE Healthcare	1:10000	WB
Anti-mouse HRP	sheep	NA931	GE Healthcare	1:10000	WB
Anti-CD3-PE	mouse	317308 (OKT3)	Biolegend	1:100	FACS
Anti-CD69-FITC	mouse	310904 (FN50)	Biolegend	1:100	FACS
Anti-CD3	mouse	317302 (OKT3)	Biolegend	1:500	T cell activation
Anti-CD28	mouse	302902 (CD28.2)	Biolegend	1:500	T cell activation
Anti-pTyr	mouse	05-321 (G418)	Millipore	1:500	IF
Anti-β-tubulin	mouse	T5293	Sigma Aldrich	1:100	WB
Anti-γ-tubulin	mouse	T6557	Sigma Aldrich	1:200	IF
Anti-Mouse-488 Alexa fluor	goat	A11001	Invitrogen	1:500	IF
Anti-Rabbit-488 Alexa fluor	goat	A11008	Invitrogen	1:500	IF
Anti-phospho Zap70 (Y493)	rabbit	2704	Cell signaling	1:1000	IF

Western Blot (WB), Immunoprecipitation (IP), Immunofluorescence (IF), Fluorescence-activated cell sorting (FACS)